The 9-1-1 DNA clamp subunit RAD1 forms specific interactions with clamp loader RAD17, revealing functional implications for binding-protein RHINO

Received for publication, October 12, 2022, and in revised form, February 18, 2023 Published, Papers in Press, February 24, 2023,
https://doi.org/10.1016/j.jbc.2023.103061

Kodai Hara (原幸大)[1], Asami Hishiki (菱木麻美)[1], Takako Hoshino (星野貴子)[1], Kiho Nagata (永田季穂)[1], Nao Iida (飯田奈央)[1], Yukimasa Sawada (澤田征昌)[1], Eiji Ohashi (大橋英治)[2], and Hiroshi Hashimoto (橋本博)[1,*]

From the [1]School of Pharmaceutical Sciences, University of Shizuoka, Shizuoka, Japan; [2]Department of Biology, Faculty of Science, Kyushu University, Fukuoka, Japan

Reviewed by members of the JBC Editorial Board. Edited by Patrick Sung

The RAD9–RAD1–HUS1 complex (9-1-1) is a eukaryotic DNA clamp with a crucial role at checkpoints for DNA damage. The ring-like structure of 9-1-1 is opened for loading onto 5′ recessed DNA by the clamp loader RAD17 RFC-like complex (RAD17–RLC), in which the RAD17 subunit is responsible for specificity to 9-1-1. Loading of 9-1-1 is required for activation of the ATR–CHK1 checkpoint pathway and the activation is stimulated by a 9-1-1 interacting protein, RHINO, which interacts with 9-1-1 *via* a recently identified RAD1-binding motif. This discovery led to the hypothesis that other interacting proteins may contain a RAD1-binding motif as well. Here, we show that vertebrate RAD17 proteins also have a putative RAD1-binding motif in their N-terminal regions, and we report the crystal structure of human 9-1-1 bound to a human RAD17 peptide incorporating the motif at 2.1 Å resolution. Our structure confirms that the N-terminal region of RAD17 binds to the RAD1 subunit of 9-1-1 *via* specific interactions. Furthermore, we show that the RAD1-binding motif of RHINO disturbs the interaction of the N-terminal region of RAD17 with 9-1-1. Our results provide deeper understanding of how RAD17–RLC specifically recognizes 9-1-1 and imply that RHINO has a functional role in 9-1-1 loading/unloading and checkpoint activation.

DNA clamps are dimeric or trimeric proteins that are conserved from bacteria to human and are even found in some phages. They form ring-shaped structures and bind DNA within their central channels. DNA clamps interact with multiple proteins involved in DNA replication, repair, and cell-cycle checkpoint, thereby stimulating their enzymatic activities and biological functions. Eukaryotes have two types of DNA clamp: homo-trimeric PCNA and hetero-trimeric 9-1-1 (RAD9–RAD1–HUS1 complex). It is generally considered that PCNA is widely involved in DNA metabolism such as DNA replication and repair (1), whereas 9-1-1 is specialized for DNA repair and DNA damage checkpoint (2, 3).

The ring structure of a DNA clamp needs to be opened to enable it to bind DNA within its central channel. Ring opening and loading of the clamp onto DNA are carried out by specialized clamp loaders, which are pentameric AAA+ ATPases (4–6). Eukaryotes have one primary loader, RFC, and three alternative loaders termed RFC-like complexes (RLCs): ATAD5–RLC, CTF18–RLC, and RAD17–RLC (7–11). In human, RFC consists of a large subunit, RFC1, and four small subunits, RFC2, RFC3, RFC4, and RFC5; these correspond in budding yeast to a large subunit, Rfc1, and four small subunits, Rfc4, Rfc5, Rfc2, and Rfc3, respectively. The alternative loaders share the four small subunits RFC2–RFC5 with RFC, but the large subunit RFC1 is replaced by a different protein (ATAD5, CTF18, or RAD17). PCNA is loaded onto 3′ recessed DNA by RFC and unloaded by ATAD5–RLC (Elg1–RLC in budding yeast). CTF18–RLC is a secondary loader of PCNA and has additional subunits (CTF8 and DCC1), thereby forming a heptameric complex. CTF18–RLC is involved in loading PCNA onto the leading strand. In contrast to PCNA, 9-1-1 is specifically and exclusively loaded onto 5′ recessed DNA by RAD17–RLC. Recent structural studies have provided novel insights into several clamp loader systems, including PCNA–RFC in human, PCNA–Rfc in budding yeast, 9-1-1–Rad24–RLC in budding yeast, and 9-1-1–RAD17–RLC in human (12–16).

The loading of 9-1-1 onto 5′ recessed DNA by RAD17–RLC is an initial step in the activation of ATR-CHK1 kinase signaling, a pathway of DNA damage checkpoint. When loaded on the 5′ recessed DNA junction, 9-1-1 interacts with multiple proteins involved in the checkpoint such as RPA, TOPBP1, ATR-ATRIP, and RHINO (17). RHINO is a tumor-related protein that was first identified in breast cancer cells (18) and subsequently characterized as a 9-1-1–binding protein involved in DNA damage checkpoint activation (19, 20). The recent crystal structure of 9-1-1 in complex with a RHINO peptide identified a RAD1-binding motif in RHINO and provided new principles of molecular interaction on DNA clamps (21). It was previously known that binding motifs for DNA clamps represented by PIP-box, a conventional PCNA-binding motif, bind to a cavity adjacent to the interdomain

* For correspondence: Hiroshi Hashimoto, hash@u-shizuoka-ken.ac.jp.

connecting–loop on the front side of the clamp (1, 22, 23). By contrast, the RAD1-binding motif of RHINO, identified as 56-WVxPxF-61 (where x is any residue), binds to a cavity around the edge-to-back side of the RAD1 subunit of 9-1-1 through van der Waals contacts, raising the possibility that other proteins besides RHINO have a RAD1-binding motif.

In this study, we identified a conserved sequence similar to the RAD1-binding motif of RHINO in the N-terminal region of RAD17, the large subunit of the 9-1-1 loader, and determined the crystal structure of human 9-1-1 bound to a RAD17 peptide incorporating the motif, thereby revealing that the N-terminal region of RAD17 binds specifically to the RAD1 subunit of 9-1-1. Furthermore, we show that the RAD1-binding motif of RHINO inhibits the interaction of the N-terminal region of RAD17 with 9-1-1. Our results provide deeper understanding of how RAD17–RLC recognizes 9-1-1 with specificity and exclusivity and furthermore have implications for 9-1-1 loading and checkpoint activation.

Results

RAD1-binding motif in RAD17

Previous work revealed that WVxPxF of RHINO is a conserved motif that binds to the edge-to-back side of RAD1 subunit of 9-1-1 in vertebrates (21). To explore whether proteins other than RHINO contain the RAD1-binding motif, we examined the amino acid sequences of proteins involved in DNA damage checkpoint in human. As a result, a sequence motif similar to the RAD1-binding motif of RHINO was identified in RAD17, the large subunit of the 9-1-1 clamp loader RAD17–RLC (Fig. 1*A*). RAD17 consists of AAA+, Collar, and A′ domains, which are conserved in the large subunit of clamp loaders and also an N-terminal region that is thought to be unstructured. We found that the putative RAD1-binding motif was located in the N-terminal region of human RAD17. Notably, the sequence is conserved within vertebrate RAD17 proteins (Fig. 1*B*) but not in RAD17 orthologs in nonvertebrates such as *Schizosaccharomyces pombe*, *Caenorhabditis elegans*, *Drosophila melanogaster*, and *Arabidopsis thaliana*. These findings strongly suggested that the conserved sequence is a RAD1-binding motif in RAD17 in vertebrates.

To explore this possibility, we crystallized human 9-1-1 in the presence of a RAD17 peptide incorporating the putative RAD1-binding motif, 16-TDWVDPSFDDF-26, and successfully determined the crystal structure of 9-1-1 in complex with this peptide at 2.1 Å resolution. The structure revealed that the RAD17 peptide does indeed bind to the cavity on the edge-to-back side of the RAD1 subunit of 9-1-1 (Fig. 2, *A* and *B*), as observed in the RHINO peptide complex (21), and indicated that vertebrate RAD17 proteins all contain a RAD1-binding motif in their N-terminal region.

Interaction of the N-terminal region of RAD17 with 9-1-1

In the structure, the bound RAD17 peptide adopts an extended conformation and specifically interacts with the cavity of the RAD1 subunit by van der Waals contacts and electrostatic interactions (Figs. 2*B* and 3*A*). The conserved hydrophobic residues, Trp18, Val19, Pro21, and Phe23, are accommodated into the cavity by van der Waals contacts with hydrophobic residues of RAD1 such as Phe64, Met256, and Phe266. These van der Waals interactions are conserved in the RHINO peptide complex (21), suggesting that they may be crucial for the association. To investigate the contribution of the hydrophobic residues within the RAD1-binding motif of

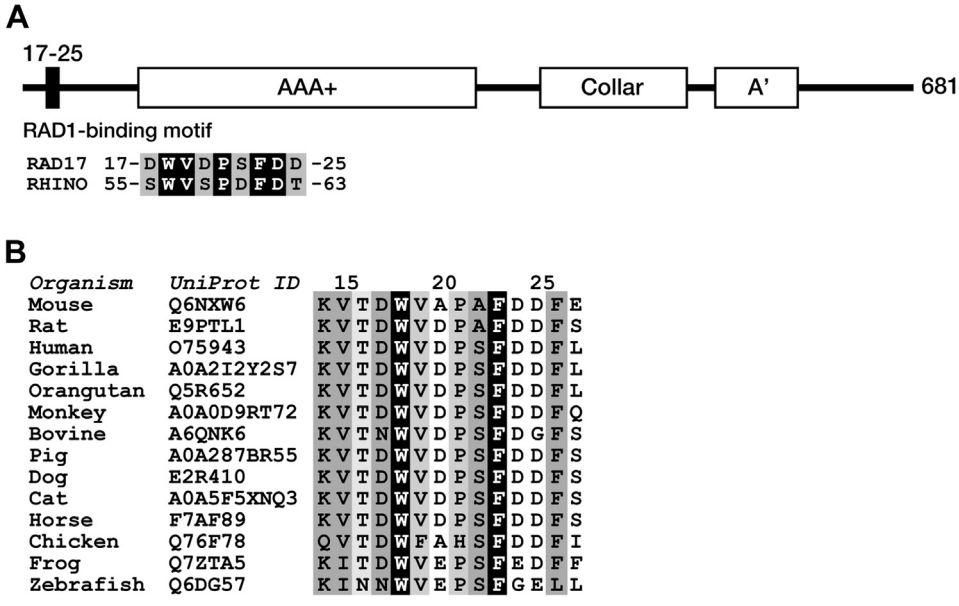

Figure 1. RAD1-biniding motif of RAD17. *A*, domain architecture of human RAD17. The RAD1-binding region (residues 17–25) is shown as a *black box*. Amino acid sequences of RAD1-binding regions of human RAD17 and RHINO are shown below the domain diagram. Identical and conserved amino acid residues are highlighted by *black* and *gray* backgrounds, respectively. *B*, amino acid sequence alignment of the N-terminal region of vertebrate RAD17 proteins. Residue numbers corresponding to human RAD17 are shown above the alignment. The degree of conservation of amino acid residues is represented in *grayscale*.

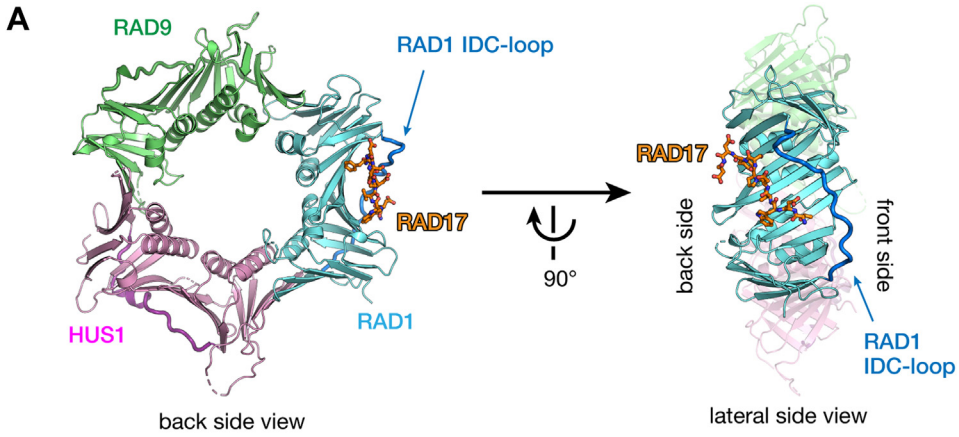

Figure 2. Structure of 9-1-1 in complex with the RAD1-binding region of RAD17. *A*, overall structure of the human 9-1-1 clamp bound to the RAD17 N-terminal peptide. The RAD9, RAD1, and HUS1 subunits are shown as *cartoon models*. The RAD17 peptide bound to RAD1 is shown as a *stick model*. The IDC-loop of RAD1 is shown as a thick tube and indicated by an *arrow*. *Left* and *right panels* show the back and lateral side views of 9-1-1, respectively. For clarification, the RAD9 and HUS1 subunits are shown as semitransparent models in the lateral side view. *B*, surface model of 9-1-1 bound to the RAD17 peptide. The RAD17 peptide is shown as a *stick model*. The IDC-loop of RAD1 is shown in *blue*. The σ-A–weighted 2*Fo*-*Fc* map of the peptide contoured at 1σ is shown as a *gray cage* in the right panel. RAD17 residues 16 to 25 are shown as a *stick model*. IDC, interdomain connecting.

RAD17 to the association with 9-1-1, an interaction analysis was performed by GST pull-down assay (Fig. 3*B*). Consistent with the present structure, the GST-fused RAD17 N-terminal fragment (RAD17N) interacted with 9-1-1. Although some nonspecific binding of 9-1-1 to GST or GS4B beads was observed, 9-1-1 strongly bound to RAD17N as compared with GST as a negative control. In contrast to RAD17N, the binding of RAD17N3A, a RAD17N variant with the triple substitution W18A/V19A/F23A, was largely reduced to the level of the negative control, indicating that these hydrophobic residues are responsible for binding through the RAD1-binding motif.

Structural comparison between the RAD17 and the RHINO peptides revealed a discrepancy in their detailed interactions with RAD1 (Fig. 3*C*). The acidic side-chain of Asp60 of RHINO is exposed to solvent and forms ionic interactions with the basic side-chains of Lys155 and Arg244 of RAD1, whereas the side-chain of Ser22 of RAD17 faces toward the cavity and forms hydrogen bonds with Ser242 and Gln254 of RAD1 (Figs. 2*B* and 3*C*). Although differences between RAD17 and RHINO were observed, their binding sites on RAD1 essentially overlapped, suggesting that RHINO might have an impact on the interaction between RAD17 and 9-1-1. In fact, in the presence of an excess amount of the RHINO peptide incorporating the RAD1-binding motif, the binding of RAD17N to 9-1-1 was reduced to a level comparable to that of GST (Fig. 3*B*). This result indicates that the binding of RHINO to 9-1-1 might interfere with the binding of RAD17–RLC to 9-1-1, possibly implying a functional role of RHINO as discussed later.

Plausible model of RAD17–RLC bound to 9-1-1

In a recent cryo-EM structure of human RAD17–RLC bound to 9-1-1 and a dsDNA-ssDNA junction, the AAA+ domain of the RAD17 subunit was observed to interact with the RAD9 subunit on the front side of the clamp, while the N-terminal 86 residues of the RAD17 subunit of the loader could not be modeled (16). Here, we built a putative structural model of RAD17–RLC bound to 9-1-1 by superimposition of the present structure and the cryo-EM structure (PDB entry 7Z6H) (16) (Fig. 4*A*). Although 61 amino acid residues between Asp25 (the C-terminus of the RAD17 peptide) and Glu87 (the N-terminus of the RAD17 subunit of the cryo-EM structure) are missing in the model, this region is sufficiently long to link Asp25 and Glu87 of RAD17 in the loader. In addition, this region is predicted to be mostly unstructured in

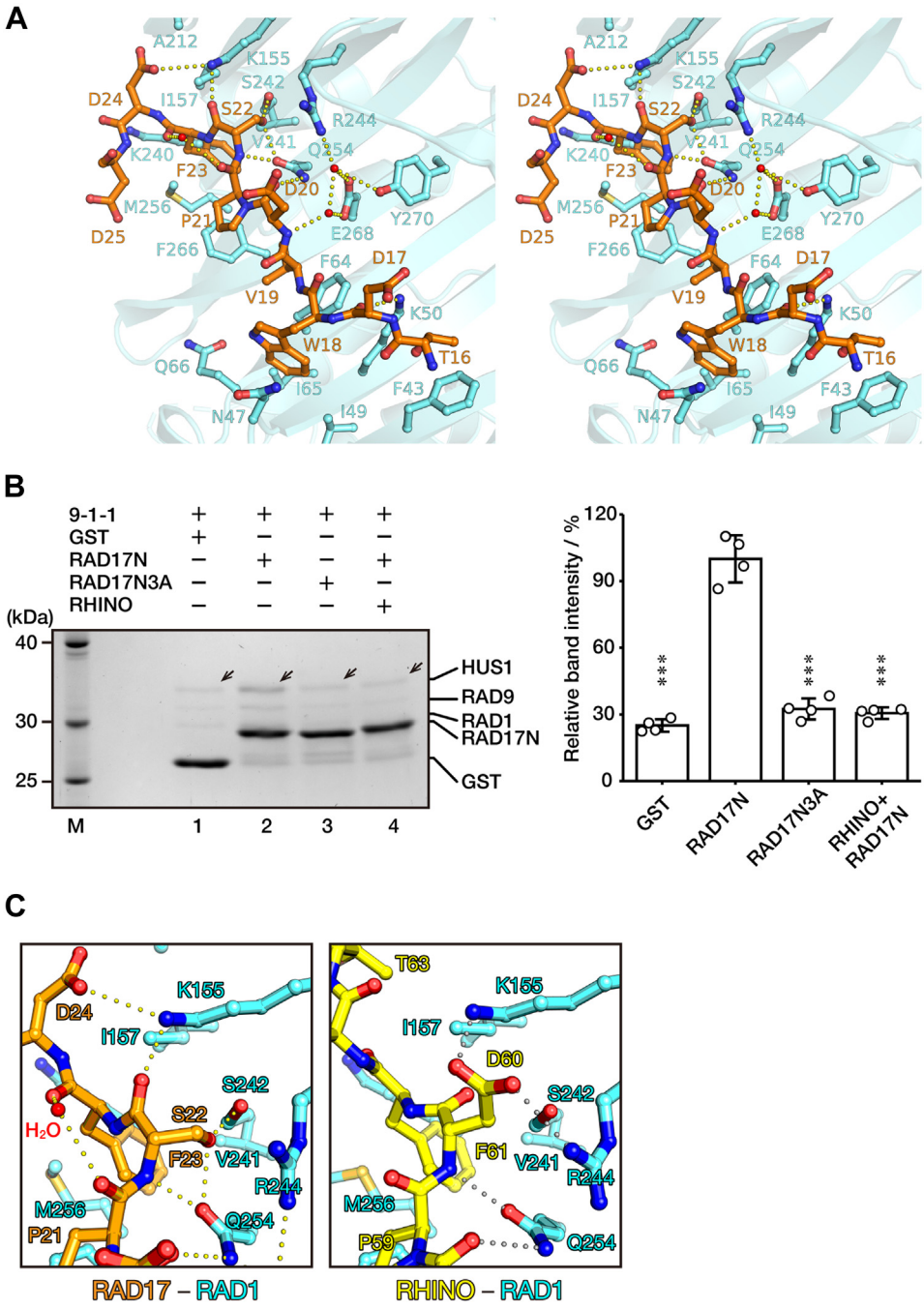

Figure 3. Interaction between RAD17 and RAD1. *A*, stereo view of the structural details of the interaction between RAD17 and RAD1. RAD17 (*orange*) is shown as a *stick model*; RAD1 (*cyan*) is shown as a cartoon model; and residues of RAD1 involved in the RAD17 interaction are shown as *stick models*. Electrostatic interactions are shown by *dots*. *B*, GST pull-down assay. *Left*, representative result of SDS-PAGE. The bands of the HUS1 subunit of 9-1-1 are indicated by *arrows*. For brevity, GST-RAD17N, GST-RAD17N3A, and RHINO peptide are abbreviated as RAD17N, RAD17N3A, and RHINO, respectively. *Right*, relative band intensities. GST, RAD17N, RAD17N3A, and RHINO+RAD17N correspond to lanes 1, 2, 3, and 4 in the *left panel*, respectively. Four independent intensities are plotted and mean values are shown as bar graphs. Error bars indicate the SDs ($n = 4$). *Asterisks* indicate statistically significant differences from RAD17N (Dunnett's test; ***$p < 0.001$). *C*, structural comparison of RAD17 (*orange*) and RHINO (*yellow*) peptides bound to the RAD1 subunit (*cyan*). RAD17–RAD1 and RHINO–RAD1 interactions are shown in the left and right panels, respectively. Electrostatic interactions are shown by *dots*.

AlphaFold DB (24) (AF-O75943-F1-model_v3). These observations suggest that our model may be a plausible structure for RAD17–RLC bound to 9-1-1, thereby demonstrating that the RAD17 subunit of the 9-1-1 loader may simultaneously interact with both the RAD9 subunit on the front side and the RAD1 subunit on the edge-to-back side of 9-1-1 (Fig. 4*A*).

Discussion

Structural basis for specificity of RAD17–RLC for 9-1-1

Recent structural studies have revealed specific interactions between the checkpoint clamp and the specialized loader (13, 14, 16). For instance, the interactions between RAD17 and RAD9 on the front side of 9-1-1 ensure exclusivity and

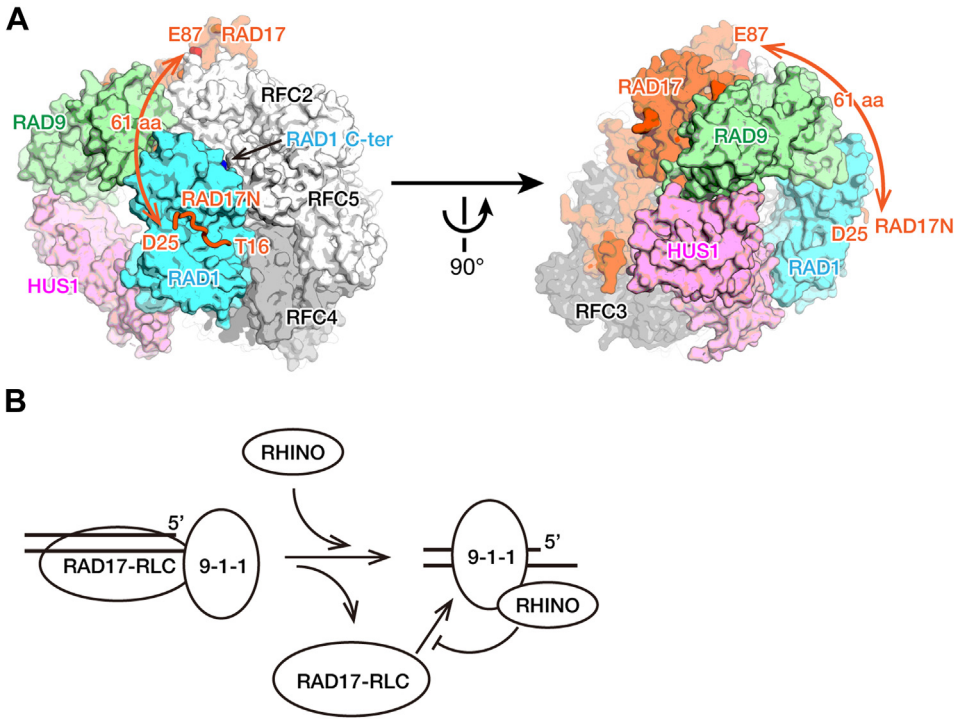

Figure 4. Functional implications for RHINO. *A*, structural model of the overall RAD17–RLC–9-1-1 interaction. 9-1-1 and RAD17–RLC, except for the N-terminal region of RAD17, are shown as surface models. The AAA+ module of RAD17-RLC interacts with the front side of 9-1-1. The N-terminal region of RAD17 bound to RAD1 is shown as an *orange tube*. Asp25 of RAD17 (the C-terminus of the RAD17 peptide in the crystal structure) and Glu87 of RAD17 (the N-terminus of the RAD17 subunit in PDB entry 7Z6H) are labeled. The *curved double arrow* shows the missing linkage of 61 amino acid residues between Asp25 and Glu87 of RAD17. The observed C-terminal end of RAD1 in the crystal structure (Asp274) is also indicated by a *black arrow*. *B*, potential function of RHINO in checkpoint activation. RHINO binds to the 9-1-1 clamp loaded on DNA, thereby probably helping to dissociate RAD17–RLC, and this might prevent RAD17–RLC from unloading 9-1-1 from DNA. RAD17-RLC, 9-1-1, RHINO are shown as *bubbles*; DNA strands shown as *straight lines*; the recessed 5′-end is labeled. RLC, RFC-like complex.

specificity in clamp selection (16) (Fig. 4*A*). The present work now reveals that RAD17 has a RAD1-binding motif and specifically binds to the RAD1 subunit on the edge-to-back side of 9-1-1. This suggests that not only the RAD17–RAD9 interaction but also the RAD17–RAD1 interaction may be involved in clamp selection. The RAD17–RAD1 interaction was not observed in the cryo-EM structure of the human RAD17–RLC–9-1-1 (16); however, the N-terminus of RAD17 was genetically fused to the C-terminus of RAD1 to stabilize the overall complex of RAD17–RLC–9-1-1. Based on the present model structure, such a modification would restrict the conformation of the N-terminal region of RAD17, thereby disturbing the inherent interaction between RAD17 and RAD1 subunits in the overall complex (Fig. 4*A*). In the cryo-EM structure, ATPγS was bound to each subunit of the RAD17–RLC, indicating that the loader might be in an active form; nevertheless, the 9-1-1 clamp was in a closed state (16). This raises the possibility that the interaction of the N-terminal region of RAD17 with the RAD1 subunit might be involved in opening of the 9-1-1 DNA clamp in vertebrates. Alternatively, an ADP-bound state of the RFC3 subunit (Rfc5 subunit in budding yeast), the so-called "E subunit", might be required to open the clamp, as observed in other clamp loader systems (12–15, 25). Further studies will be required to elucidate the detailed mechanisms underlying the opening of 9-1-1 by RAD17–RLC in vertebrates.

Implications for the function of RHINO in checkpoint activation

The present study has revealed that the RAD17-binding site on RAD1 overlaps with the RHINO-binding site on RAD1 and that a RHINO peptide incorporating the RAD1-binding motif interferes with the interaction between the N-terminal region of RAD17 and 9-1-1. It has been reported that the RAD1-binding motif of RHINO is involved in activation of the ATR–CHK1 pathway (19). Therefore, it seems likely that the RHINO–RAD1 interaction occurs after 9-1-1 is loaded onto DNA by RAD17–RLC. Based on that consideration, we could speculate a potential function of RHINO (Fig. 4*B*). In response to DNA damage, 9-1-1 is first loaded onto recessed 5′ DNA by RAD17–RLC. Subsequently, RAD17–RLC would be dissociated from the loaded 9-1-1 in a step that might be facilitated by RHINO through its interaction with the RAD1 subunit of 9-1-1. Furthermore, the RHINO–RAD1 interaction might disturb unloading of the loaded 9-1-1 clamp by RAD17–RLC, possibly facilitating the assembly of checkpoint proteins. In other words, RHINO might be involved in checkpoint activation by retaining or stabilizing the loaded 9-1-1 on DNA. Further studies by biochemical and structural approaches will be needed to validate the proposed model and to elucidate the detailed mechanism of 9-1-1 loading in vertebrates, as well as the function of RHINO in DNA damage checkpoint. These are the subjects of our future studies.

Experimental procedures

Crystallization and structure determination

Recombinant human 9-1-1 was prepared by a procedure based on a previously reported protocol (21). In brief, the C-terminal–truncated RAD9 (residues 1–270), N-terminal His-tag–fused HUS1, and RAD1 were coexpressed by *Escherichia coli* BL21(DE3) with IPTG induction. The 9-1-1 was purified by HiTrap Heparin, HiTrap Q, and HiLoad Superdex200 columns (Cytiva). Purified protein was concentrated, frozen in liquid nitrogen, and stored at 193 K until use. The human RAD17 peptide (16-TDWVDPSFDDF-26) was commercially synthesized (Toray Research Center, Inc) and dissolved in a buffer (20 mM Hepes–NaOH pH 7.4 and 100 mM NaCl). A 10-fold molar excess of the peptide was incubated with 0.13 mM 9-1-1 at 277 K overnight. Crystallization was performed by the vapor-diffusion method. Rod crystals were obtained with a reservoir solution of 0.1 M Bis-Tris propane pH 7.5, 0.1 M sodium citrate, and 16% PEG 3350 at 293 K. Crystals were transferred to a buffer containing the reservoir solution and 20% glycerol. X-ray diffraction data were collected at Photon Factory beamline BL-17A with an EIGER X16M single photon counting detector (DECTRIS). Diffraction data were processed with the programs XDS (26) and PHENIX (27). The crystal structure of 9-1-1 bound to the RAD17 peptide was determined by the molecular replacement method using the program PHASER (28). The structure of 9-1-1 bound to RHINO peptide (21) (PDB entry 6J8Y) was used as the search model of molecular replacement. Binding of the RAD17 peptide to the RAD1 subunit was clearly observed in the electron density map, and the structure of peptide was built by the program Coot (29). The structure was improved and refined by the programs Coot (29) and PHENIX (27). Data collection and refinement statistics are given in Table 1.

Table 1
Data collection and refinement statistics

Data collection	
Space group	$P2_12_12_1$
Cell dimensions	53.18 136.30 154.04
Resolution (Å)	20.00–2.12 (2.24–2.12)
R-merge/*R*-meas	0.067 (0.916)/0.073 (0.887)
$I/\sigma I$	18.3 (2.1)
CC 1/2	0.999 (0.761)
Completeness (%)	99.9 (99.6)
No. total/unique reflections	435,477 (43,520)/64,368 (6285)
Multiplicity	6.8 (6.9)
Wilson B-factor (Å^2)	40.42
Refinement	
Resolution (Å)	19.81–2.12 (2.20–2.12)
No. refined/free reflections	
R-work/*R*-free	0.2174 (0.3057)/0.2625 (0.3639)
No. atoms	
9-1-1/RAD17 peptide/Water	6210/84/252
Averaged B-factors (Å^2)	
9-1-1/RAD17 peptide/Water	48.97/57.19/48.81
RMS deviations	
Bond lengths (Å)/angles (°)	0.004/0.77
Ramachandran Plot	
Favored (%)	97.43
Allowed (%)	2.57
Outliers (%)	0
PDB entry	8GNN

Values in parentheses are for highest resolution shell.

Atomic coordinates and structure-factor amplitudes have been deposited in the Protein Data Bank (PDB entry 8GNN).

Pull-down assay

GST or GST-fused human RAD17 (residues 16–28) termed GST-RAD17N was expressed by *E. coli* BL21(DE3) by conventional induction with IPTG. The cells were disrupted in buffer I (20 mM Hepes–NaOH pH 7.4 and 500 mM NaCl) by sonication on ice and then the cell lysate was clarified by centrifugation for 45 min at 277 K (48,000*g*). The supernatant was incubated with GS4B beads (Cytiva) at 277 K overnight. The beads were washed with buffer II (20 mM Hepes–NaOH pH 7.4 and 2.0 M NaCl) and then washed with buffer III (20 mM Tris–HCl pH 8.5 and 100 mM NaCl). The bound protein was eluted with buffer IV (20 mM Tris–HCl pH 8.5, 100 mM NaCl, 30 mM reduced glutathione, and 10 mM $MgCl_2$). The eluent was dialyzed with buffer V (20 mM Hepes–NaOH pH 7.4 and 100 mM NaCl). Aliquots of the purified protein were stored at 193 K until use. The triple substitutions W18A/V19A/F23A in GST-RAD17N were introduced by a PCR-based mutagenesis. GST-RAD17N with the triple substitutions termed GST-RAD17N3A was prepared by a procedure similar to that of GST-RAD17N.

GST (0.250 nmol), GST-RAD17N (0.250 nmol), or GST-RAD17N3A (0.250 nmol) was incubated with 9-1-1 (1.00 nmol) at 277 K overnight and then incubated with GS4B beads (50 μl) at 277 K for 75 min. The beads were washed with buffer V including 0.1 v/v% Tween-20 three times. The bound proteins were eluted with buffer IV and analyzed by SDS-PAGE with CBB-staining. Analysis of SDS-PAGE was independently performed four times. The band intensities were quantified by a ChemiDoc Touch imaging system (Bio-Rad Laboratories, Inc). The relative band intensity of HUS1 divided by the band intensity of GST or GST-RAD17N3A was normalized to that of GST-RAD17N. In competition assay between RAD17 and RHINO, the RHINO peptide including the RAD1-binding motif (54-TSWVSPDFDTA-64) (Toray Research Center, Inc) was used. The RHINO peptide was dissolved with buffer V. Purified 9-1-1 (1.00 nmol) was incubated with the RHINO peptide (12.5 nmol) on ice for 30 min and then incubated with GST-RAD17N (0.250 nmol) at 277 K overnight. The following experiment and analysis were performed with a procedure mentioned above.

Data availability

The coordinates for the 9-1-1 bound to the RAD17 peptide are deposited with the Protein Data Bank, accession code 8GNN. All other data are within the manuscript.

Acknowledgments—We thank the beamline staff of Photon Factory for kind support in data collection.

Author contributions—K. H., A. H., and H. H. methodology; K. H., A. H., T. H., K. N., N. I., and Y. S. investigation; K. H., A. H., T. H., K. N., N. I., Y. S., E. O., and H. H. data curation; H. H. writing–original

draft; K. H., A. H., E. O., and H. H. writing–review and editing; E. O. resources; H. H. conceptualization; H. H. supervision.

Funding and additional information—This work was supported by Grants-in-Aid for Scientific Research (KAKENHI) from Japan Society for the Promotion of Science (JSPS) to H. H. (16H04755 and 17H06014) and to K. H. (20H03197 and 21H05757) and a grant from the Protein Research Foundation to K. H. The Takeda Science Foundation and Naito Foundation also supported the activities of H. H. in this work.

Conflict of interest—The authors declare that they have no conflicts of interest with the contents of this article.

Abbreviations—The abbreviations used are: IDC, interdomain connecting; RLC, RFC-like complex.

References

1. Moldovan, G. L., Pfander, B., and Jentsch, S. (2007) PCNA, the maestro of the replication fork. *Cell* **129**, 665–679
2. Eichinger, C. S., and Jentsch, S. (2011) 9-1-1: PCNA's specialized cousin. *Trends Biochem. Sci.* **36**, 563–568
3. Parrilla-Castellar, E. R., Arlander, S. J., and Karnitz, L. (2004) Dial 9-1-1 for DNA damage: the Rad9-Hus1-Rad1 (9-1-1) clamp complex. *DNA Rep.* **3**, 1009–1014
4. Mossi, R., and Hübscher, U. (1998) Clamping down on clamps and clamp loaders–the eukaryotic replication factor C. *Eur. J. Biochem.* **254**, 209–216
5. Kelch, B. A., Makino, D. L., O'Donnell, M., and Kuriyan, J. (2012) Clamp loader ATPases and the evolution of DNA replication machinery. *BMC Biol.* **10**, 34
6. Shiomi, Y., and Nishitani, H. (2017) Control of genome integrity by RFC complexes; conductors of PCNA loading onto and unloading from chromatin during DNA replication. *Genes* **8**, 52
7. Kim, J., and MacNeill, S. A. (2003) Genome stability: a new member of the RFC family. *Curr. Biol.* **13**, R873–R875
8. Kupiec, M. (2016) Alternative clamp loaders/unloaders. *FEMS Yeast Res.* **16**, fow084
9. Ohashi, E., and Tsurimoto, T. (2017) Functions of multiple clamp and clamp-loader complexes in eukaryotic DNA replication. *Adv. Exp. Med. Biol.* **1042**, 135–162
10. Lee, K.,Y., and Park, S. H. (2020) Eukaryotic clamp loaders and unloaders in the maintenance of genome stability. *Exp. Mol. Med.* **52**, 1948–1958
11. Arbel, M., Choudhary, K., Tfilin, O., and Kupiec, M. (2021) PCNA loaders and unloaders-one ring that rules them all. *Genes* **12**, 1812
12. Gaubitz, C., Liu, X., Magrino, J., Stone, N. P., Landeck, J., Hedglin, M., *et al.* (2020) Structure of the human clamp loader reveals an autoinhibited conformation of a substrate-bound AAA+ switch. *Proc. Natl. Acad. Sci. U. S. A.* **117**, 23571–23580
13. Castaneda, J. C., Schrecker, M., Remus, D., and Hite, R. K. (2022) Mechanisms of loading and release of the 9-1-1 checkpoint clamp. *Nat. Struct. Mol. Biol.* **29**, 369–375
14. Zheng, F., Georgescu, R. E., Yao, N. Y., O'Donnell, M. E., and Li, H. (2022) DNA is loaded through the 9-1-1 DNA checkpoint clamp in the opposite direction of the PCNA clamp. *Nat. Struct. Mol. Biol.* **29**, 376–385
15. Gaubitz, C., Liu, X., Pajak, J., Stone, N. P., Hayes, J. A., Demo, G., *et al.* (2022) Cryo-EM structures reveal high-resolution mechanism of a DNA polymerase sliding clamp loader. *Elife* **11**, e74175
16. Day, M., Oliver, A. W., and Pearl, L. H. (2022) Structure of the human RAD17-RFC clamp loader and 9-1-1 checkpoint clamp bound to a dsDNA-ssDNA junction. *Nucleic Acids Res.* **50**, 8279–8289
17. Maréchal, A., and Zou, L. (2013) DNA damage sensing by the ATM and ATR kinases. *Cold Spring Harb. Perspect. Biol.* **5**, a012716
18. Kim, J. W., Fukukawa, C., Ueda, K., Nishidate, T., Katagiri, T., and Nakamura, Y. (2010) Involvement of C12orf32 overexpression in breast carcinogenesis. *Int. J. Oncol.* **37**, 861–867
19. Cotta-Ramusino, C., McDonald, E. R., 3rd, Hurov, K., Sowa, M. E., Harper, J. W., and Elledge, S. J. (2011) A DNA damage response screen identifies RHINO, a 9-1-1 and TopBP1 interacting protein required for ATR signaling. *Science* **332**, 1313–1317
20. Lindsey-Boltz, L. A., Kemp, M. G., Capp, C., and Sancar, A. (2015) RHINO forms a stoichiometric complex with the 9-1-1 checkpoint clamp and mediates ATR-Chk1 signaling. *Cell Cycle* **14**, 99–108
21. Hara, K., Iida, N., Tamafune, R., Ohashi, E., Sakurai, H., Ishikawa, Y., *et al.* (2020) Structure of the RAD9-RAD1-HUS1 checkpoint clamp bound to RHINO sheds light on the other side of the DNA clamp. *J. Biol. Chem.* **295**, 899–904
22. Mailand, N., Gibbs-Seymour, I., and Bekker-Jensen, S. (2013) Regulation of PCNA-protein interactions for genome stability. *Nat. Rev. Mol. Cell. Biol.* **14**, 269–282
23. Hashimoto, H., Hara, K., Hishiki, A., and June 22. (2022) Structural basis for molecular interactions on the eukaryotic DNA sliding clamps PCNA and RAD9-RAD1-HUS1. *J. Biochem.* **172**, 189–196
24. Jumper, J., Evans, R., Pritzel, A., Green, T., Figurnov, M., Ronneberger, O., *et al.* (2021) Highly accurate protein structure prediction with AlphaFold. *Nature* **596**, 583–589
25. Kelch, B. A., Makino, D. L., O'Donnell, M., and Kuriyan, J. (2011) How a DNA polymerase clamp loader opens a sliding clamp. *Science* **334**, 1675–1680
26. Kabsch, W. (2010) XDS. *Acta Crystallogr. D Biol. Crystallogr.* **66**, 125–132
27. Adams, P. D., Afonine, P. V., Bunkóczi, G., Chen, V. B., Davis, I. W., Echols, N., *et al.* (2010) PHENIX: a comprehensive Python-based system for macromolecular structure solution. *Acta Crystallogr. D Biol. Crystallogr.* **66**, 213–221
28. McCoy, A. J., Grosse-Kunstleve, R. W., Adams, P. D., Winn, M. D., Storoni, L. C., and Read, R. J. (2007) Phaser crystallographic software. *J. Appl. Crystallogr.* **40**, 658–674
29. Emsley, P., Lohkamp, B., Scott, W. G., and Cowtan, K. (2010) Features and development of Coot. *Acta Crystallogr. D Biol. Crystallogr.* **66**, 486–501